Short Article

Cell Stem Cell

Ground State Conditions Induce Rapid Reorganization of Core Pluripotency Factor Binding before Global Epigenetic Reprogramming

Graphical Abstract

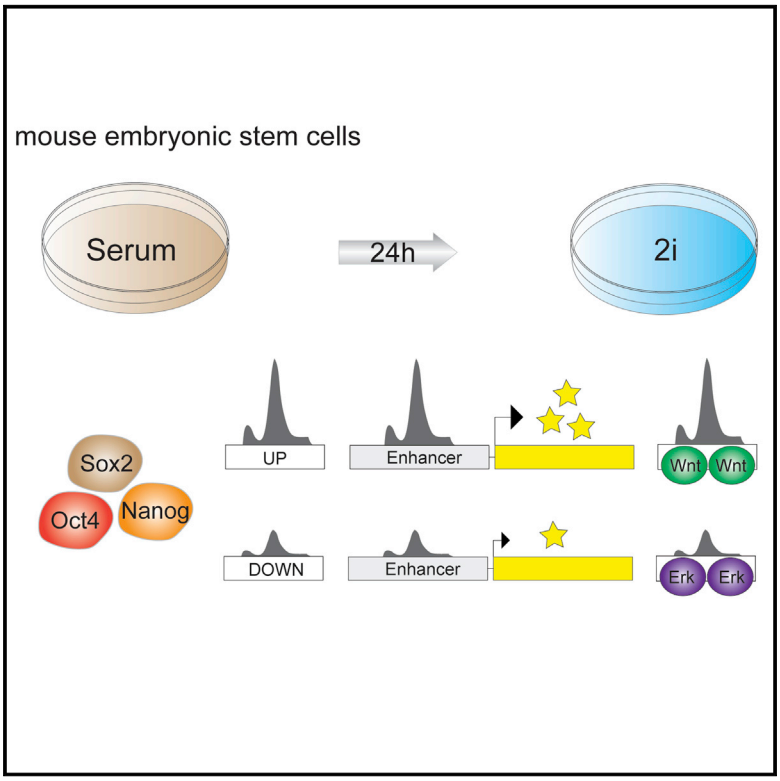

Authors

Christina Galonska, Michael J. Ziller, Rahul Karnik, Alexander Meissner

Correspondence

alexander_meissner@harvard.edu

In Brief

Meissner and colleagues provide a comprehensive characterization of the early OCT4, SOX2, and NANOG binding dynamics during the transition from serum/LIF to 2i. The target rewiring predominantly affects distal regulatory elements with a plausible link to the upstream signaling pathways. Notably, these events appear before any major epigenetic reprogramming events, which occur only later in the transition.

Highlights

- Early and widespread reconfiguration of OCT4, SOX2, and NANOG binding in 2i
- Differential OSN binding correlates with enhancer activity in 2i
- Dynamic targets show co-occurring motifs of factors linked to Wnt and Erk signaling
- PRC2 appears dispensable for continued silencing and de novo repression in 2i

Accession Numbers

GSE56312

Galonska et al., 2015, Cell Stem Cell *17*, 462–470
October 1, 2015 ©2015 Elsevier Inc.
http://dx.doi.org/10.1016/j.stem.2015.07.005

CellPress

Cell Stem Cell
Short Article

Ground State Conditions Induce Rapid Reorganization of Core Pluripotency Factor Binding before Global Epigenetic Reprogramming

Christina Galonska,[1,2,3,4] Michael J. Ziller,[1,2,3,4] Rahul Karnik,[1,2,3] and Alexander Meissner[1,2,3,*]
[1]Broad Institute of MIT and Harvard, Cambridge, MA 02142, USA
[2]Harvard Stem Cell Institute, Cambridge, MA 02138, USA
[3]Department of Stem Cell and Regenerative Biology, Harvard University, Cambridge, MA 02138, USA
[4]Co-first author
*Correspondence: alexander_meissner@harvard.edu
http://dx.doi.org/10.1016/j.stem.2015.07.005

SUMMARY

Mouse embryonic stem cells (mESCs) cultured under serum/LIF conditions exhibit heterogeneous expression of pluripotency-associated factors that can be overcome by two inhibitors (2i) of the MEK and GSK3 pathways. Several studies have shown that the "ground state" induced by 2i is characterized by global hypomethylation and specific transcriptional profiles, but little is known about the contributing effectors. Here we show that 2i conditions rapidly alter the global binding landscape of OCT4, SOX2, and NANOG. The dynamic binding influences enhancer activity and shows enrichment for regulators linked to Wnt and Erk signaling. Epigenomic characterization provided limited insights to the immediate transcriptional dynamics, suggesting that these are likely more secondary effects. Likewise, loss of the PRC2 component EED to prevent H3K27me3 deposition had minimal effect on the transcriptome, implying that it is largely dispensable for continued repression of bivalent genes and de novo silencing in 2i.

INTRODUCTION

Under common culture conditions in serum plus Leukemia Inhibitory Factor (LIF), mouse embryonic stem cells (ESCs) receive partially opposing signaling cues, as serum/LIF-induced STAT3 signaling favors the pluripotent state, but does not block the activation of Fgf/Erk signaling involved in cellular differentiation (Kunath et al., 2007). To suppress these differentiation cues, mESCs can be maintained in the absence of serum using defined conditions that include two kinase inhibitors (2i) (Ying et al., 2008). PD0325901 (PD) inhibits the function of mitogen-activated protein kinase kinase (MAPKK), thereby inhibiting the Erk signaling cascade, and CHIR99021 (CHIR) selectively targets glycogen synthase kinase-3 (GSK3), resulting in an enforcement of canonical Wnt signaling. This "2i state" of so-called naive pluripotency has been shown to be very distinct in its transcriptional and epigenetic profiles from ESCs cultured in serum/LIF (Habibi et al., 2013; Marks et al., 2012). The state is marked by the specific upregulation of genes involved in metabolism and stem cell maintenance, while developmental- and differentiation-associated genes become more repressed (Marks et al., 2012). The observed differences in the transcriptional state further coincide with drastic changes in the epigenetic landscape of the cells, i.e., a reduction of H3K27me3 at bivalent gene promoters and a global loss of DNA methylation (Ficz et al., 2013; Habibi et al., 2013; Marks et al., 2012).

Another hallmark of the 2i transition is the more homogenous distribution of NANOG protein, switching from fluctuating (lower and higher) levels under serum conditions to increased expression and more uniform protein distribution under 2i conditions (Silva et al., 2009), pointing to a possible stabilization and reinforcement of the core pluripotency circuitry in 2i. Although it is known that the pluripotent state is highly dependent on the intrinsic gene regulatory network centered around the core pluripotency factors OCT4, SOX2, and NANOG (OSN) (Chen et al., 2008; Kim et al., 2008) and that cell state transitions involve the remodeling of the core network (Buecker et al., 2014; Chan et al., 2013), little is known about the specific impact that the two inhibitors have on the OSN target spectrum.

Given the broad interest in the 2i state and the dramatic cellular state changes that are induced through the inhibitors, we decided to investigate the effects on OSN binding and study their behavior early under the distinct culture conditions. To capture putative regulatory events upstream of major transcriptional and epigenetic dynamics, we focused on mESCs 24 hr after the switch (serum/LIF to 2i/LIF, hereafter referred as "serum" and "2i") and measured gene expression, DNA methylation, selected histone modifications, and OSN binding. Integrative analysis of this multi-layered dataset together with select functional validation experiments including enhancer activity assays and PRC2 mutant ESCs provides new mechanistic insights that advance our understanding of this unique cellular state.

RESULTS

Reorganization of Core Pluripotency Factor Binding in the Early 2i Transition

Several recent studies have highlighted the transcriptional and epigenetic dynamics between cells in serum versus 2i (Ficz et al., 2013; Marks et al., 2012). Notably, the induction

and repression of selected factors (e.g., *Prdm14* and *Dnmt3a/3b*) has been reported as early as 24 hr after addition of the two inhibitors, pointing to a rapid transition of the ESC transcriptome (Ficz et al., 2013). Using RNA sequencing we were able to identify 1,013 genes that significantly changed their expression in the initial 2i transition (24 hr 2i) and partially overlapped with the 1,413 altered genes in the 2i population after three passages (3P) (Figure S1A, Table S1). We grouped the differentially expressed genes across all three conditions into six clusters (Figure 1A, Figure S1B). This clustering captures recently described dynamics such as the downregulation of *Otx2* and the upregulation of *Klf2* (Yang et al., 2014; Yeo et al., 2014). Genes with moderate but not yet significant expression changes in the initial transition (cluster 2 and 5) encompass factors such as *Prdm14* and *Eras*, which become highly divergent later in the transition (Figure S1B). Overall, nearly half of the genes that become repressed in 2i and a quarter of genes that become upregulated in 2i already show altered expression within the first 24 hr (Figure 1B). *Oct4* and *Sox2* show little expression change upon switching conditions, while *Nanog* expression increases by around 1.5-fold (Figure S1C). It is worth noting that besides *Nanog*, we find several other pluripotency-related genes that are differentially expressed in the initial 2i transition, including *Dppa3* and *Utf1* at the extremes (Figure 1C). Utilizing our previously established *Utf1*-mCitrine reporter line (Galonska et al., 2014), we confirmed that *Utf1* is rapidly and uniformly repressed upon being switched to 2i (Figure 1D). Additionally, STELLA and NANOG appear more homogenously distributed across the population already within the first 24 hr in 2i (Figure 1E).

To gain more mechanistic insights into the early regulatory events, we analyzed the genome-wide binding patterns of OSN under both conditions. To be able to quantify both new and altered binding patterns, we utilized established, state-of-the-art analytical methods, based on a negative-binomial model and variance pooling as implemented in the publically available software packages diffbind (http://bioconductor.org/packages/release/bioc/html/DiffBind.html) and DESeq2 (http://bioconductor.org/packages/release/bioc/html/DESeq2.html). Using this approach, we find that all three factors become subject to widespread binding rearrangements, with 14,796 sites exhibiting differential NANOG binding, 1,352 sites with differential SOX2 binding, and 503 sites with differential OCT4 binding with a minimal 2-fold change at a false discovery rate (FDR) of 0.1 (NANOG and SOX2) or a $p \leq 0.05$ (OCT4) (Figure 1F, Table S2). Clustering these regions reveals mostly coordinated binding changes for all three factors (Figure 1F). It should be noted that many of the observed binding changes were subtler for OCT4 and SOX2, thereby frequently falling below our threshold criteria for differential binding sites (Figure 1F, Figure S1D). Importantly, the majority of differentially enriched NANOG and SOX2 binding sites are shared between 24 hr and 3P (Figure S1E), suggesting that early binding changes are largely maintained. Gene ontology analysis shows that differentially bound sites are enriched for biological processes associated with development and differentiation (Table S3), in line with OSN's known targeting of developmental genes in serum (Kim et al., 2008).

Analysis of H3K4me3 and H3K27me3 patterns showed that the majority of genomic sites with altered OSN binding are distinct from the sites that show dynamics for these two histone modifications (Figure 1F). This observation is largely expected based on our observations that the core pluripotency factors are more frequently found at distal putative regulatory sites (Gifford et al., 2013; Ziller et al., 2013), while H3K4me3 and H3K27me3 can be found primarily at promoters or intragenic regions (Figure 1G). While initially less dynamic, H3K4me3 and H3K27me3 are further reorganized at later stages of the transition (Figure S1F). To evaluate if the observed OSN binding changes in 2i are indeed state-specific rather than the result of transitioning to a more homogenous cell population, we utilized a NANOG GFP reporter line whose serum population consists of a heterogeneous mixture of GFP-negative and GFP-positive cells. Next, we isolated the GFP-positive population in serum (Figure S1G) and compared its NANOG binding pattern to that of the 2i population. Although a fraction of binding sites changed between the whole serum population and the GFP-positive subpopulation, the global rewiring that occurs in the 2i transition was not seen. Thus, the GFP-positive fraction exhibited equally many binding changes to the 2i state as the whole serum population (Figure S1H). This is in agreement with previous results showing that the transcriptome of REX1-positive sorted serum cells is still highly divergent from the homogenous REX1-positive 2i population (Marks et al., 2012).

Lastly, to assess the effect of the reconfigured binding on transcription in more detail, we correlated differential binding with expression of the nearest gene ($\leq$50Kb of transcriptional start site [TSS]). A large fraction of all differentially expressed genes in 2i are bound by at least one of the three factors in serum (Figure S1I). Specifically, 46% of all upregulated genes and 29% of all downregulated genes exhibit a differential OSN binding pattern after 24 hr in 2i (Figure 1H). However, considering the number of differentially bound sites and differentially expressed genes, this association is not statistically significant in all cases: while genes repressed upon transition to 2i were enriched for OSN sites that show decreased binding in 2i, upregulated genes were equally enriched for sites with lower and higher OSN binding (Figure S1J).

Differentially Bound Sites Are Enriched at Distal Gene Regulatory Elements

Our analysis points toward an enrichment of dynamic regions at distal putative regulatory sites, which is in line with two recent studies showing that the transition to alternative pluripotent states (e.g., 2i to EpiSCs) is accompanied by remodeling of the cellular enhancer landscape (Buecker et al., 2014; Factor et al., 2014). A well-known example for differential enhancer use in primed versus naive pluripotency is the switch from the *Oct4* proximal (serum) to the distal (2i) element (Tesar et al., 2007). Although we do not observe a complete switch in binding between these elements, we find that the proximal enhancer shows decreased NANOG binding upon being switched to 2i, while the distal enhancer showed a small increase in SOX2 (Figure 2A).

To determine the possible effects of differential binding, we first assessed the activity of several enhancer elements in serum and 2i using a luciferase-based reporter assay. As expected, the proximal enhancer shows diminished activity in 2i, while the distal enhancer element clearly gained activity (Figure 2B). We then

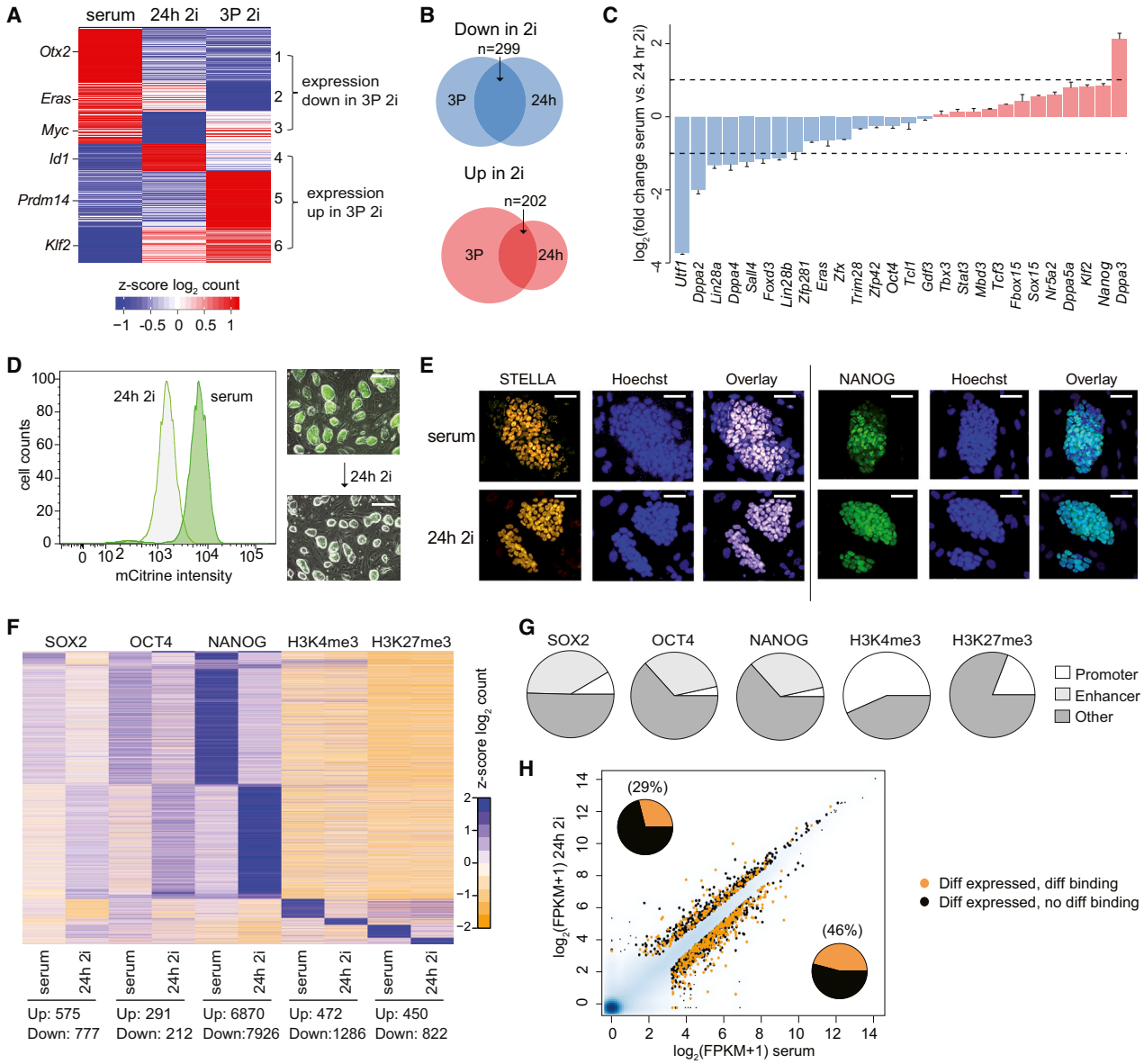

Figure 1. Globally Reconfigured Binding of the Core Pluripotency Factors in the Early 2i Transition

(A) Expression data (z score $\log_2$ count) for cells cultured in serum, 24 hr 2i, or three passages 2i (3P). Only genes with FPKM > 1 in at least one of the conditions are shown.

(B) Venn diagrams showing the overlap between all significantly downregulated and upregulated genes in 24 hr 2i versus serum as compared to 3P 2i versus serum. We find an overlap of 299 downregulated genes (47% relative to 3P set) and 202 upregulated genes (26% relative to 3P set) between 24 hr in 2i and 3P in 2i. Diagrams are drawn to scale.

(C) Expression ($\log_2$ fold change) of pluripotency-associated transcription factors in serum versus 24 hr 2i. The error bars represent one SE over two biological replicates.

(D) FACS sorting showing the fluorescent intensity of Utf1-mCitrine reporter cells in serum versus 24 hr 2i. On the right: images of the reporter cell line in serum and after switching cells to 24 hr 2i. Scale bar, 150 μm.

(E) Immunofluorescent pictures of STELLA and NANOG in serum versus 24 hr 2i. Protein distributions of STELLA and NANOG become more homogenous after 24 hr in 2i. Scale bar, 80 μm.

(F) Heatmap showing all differential binding sites (z score $\log_2$ count) for SOX2, OCT4, NANOG, H3K4me3, and H3K27me3 in serum and 24 hr 2i. Numbers of more highly (up) and less (down) enriched sites are shown below.

(G) Pie charts illustrating the proportion of differentially enriched SOX2, OCT4, NANOG, H3K4me3, and H3K27me3 sites that overlap with promoters (±1 kb of TSS) or enhancers based on previously published p300 binding sites in mESCs in serum (Creyghton et al., 2010). All regions not overlapping with either one of these two were classified as other regions.

(H) Scatterplot showing all significantly up- and downregulated genes after 24 hr 2i that are (orange dots) or are not (black dots) differentially bound by OCT4, SOX2, or NANOG. 29% of the upregulated genes in 2i become differentially bound by the core factors (left pie chart) and 46% of all downregulated genes in 2i become differentially bound by the core factors (right pie chart).

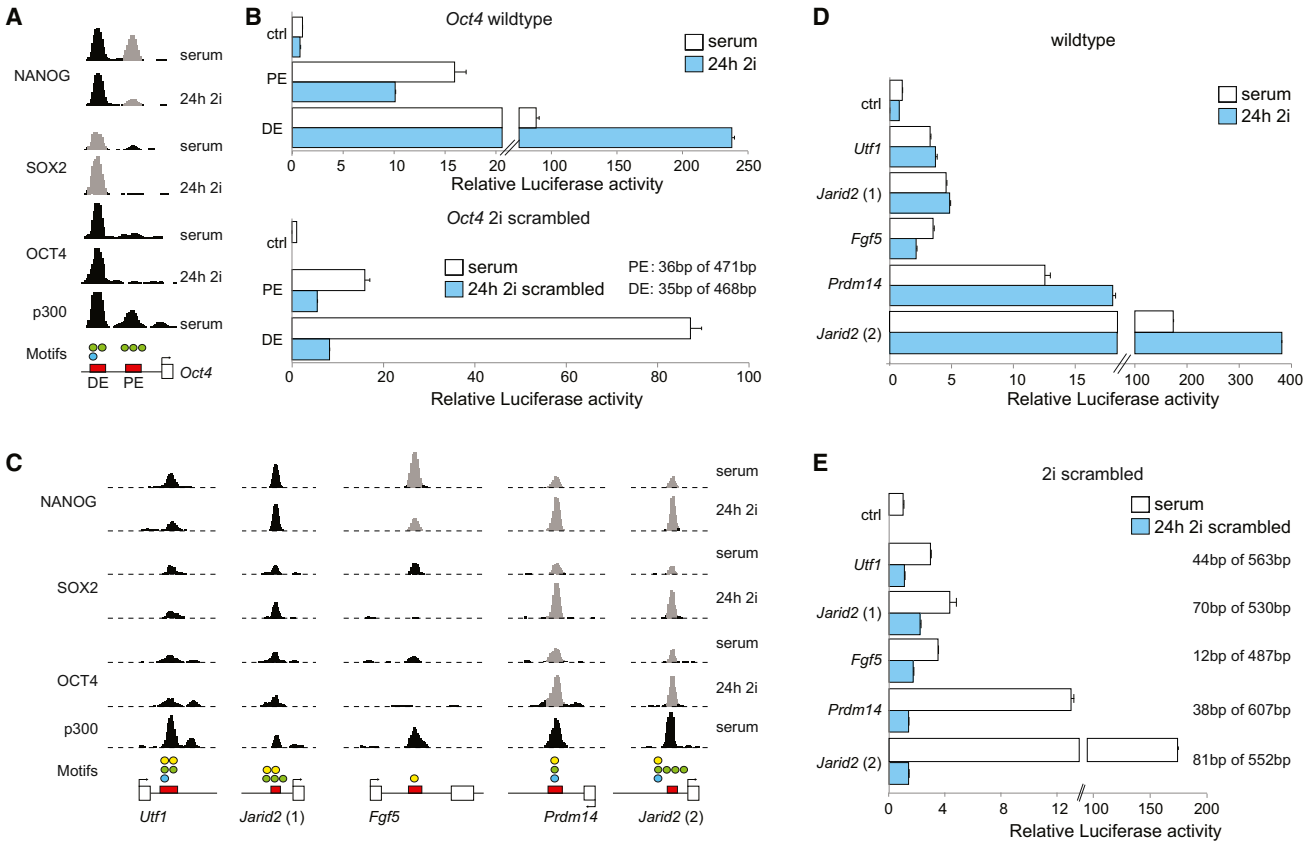

Figure 2. Differential OSN Binding Can Be Linked to Differential Enhancer Activity in 2i

(A) ChIP-seq tracks showing the binding of NANOG, SOX2, OCT4, and p300 in serum and 24 hr 2i (p300 only in serum) along the *Oct4* proximal (PE) and distal (DE) enhancer elements. Serum and 24 hr 2i ChIP-seq tracks are scaled to the same height for each factor and locus. Differentially bound regions for NANOG and SOX2 are highlighted in gray. Regions tested in the luciferase assay (B) are displayed as red boxes. Presence of OSN binding motifs are indicated as circles. Green circles, SOX2; blue circles, OCT4. Number of circles indicates the frequency of the motif.

(B) Top: relative Luciferase activity of the *Oct4* proximal (PE) and distal (DE) enhancer elements in serum and 24 hr 2i (n = 3). The empty pGL4.24 plasmid (Promega) was used as control (ctrl). Bottom: relative Luciferase activity of the *Oct4* proximal (PE) and distal (DE) enhancer elements in serum as compared to the scrambled elements in 24 hr 2i. The empty pGL4.24 plasmid (Promega) was used as control (ctrl). The number of scrambled nucleotides targeting the OSN motifs and total length of the total tested elements are shown on the right. Error bars represent one SD over three technical replicates.

(C) ChIP-seq tracks showing the binding of NANOG, SOX2, OCT4, and p300 along the *Utf1*, *Jarid2* (enhancer 1 and 2), *Fgf5*, and *Prdm14* enhancer elements in serum and 24 hr 2i (p300 only in serum). Serum and 24 hr 2i ChIP-seq tracks are scaled to the same height for each factor and locus. Regions tested in the luciferase assay (D and E) are displayed as red boxes. Differentially bound regions for NANOG, SOX2, and OCT4 are highlighted in gray. Presence of OSN binding motifs are indicated as circles. Green circles, SOX2; blue circles, OCT4; and yellow circles, NANOG. Number of circles indicates the frequency of the motif.

(D) Relative Luciferase activity of the *Utf1*, *Jarid2* (enhancer 1 and 2), *Fgf5*, and *Prdm14* enhancer elements in serum and 24 hr 2i. The empty pGL4.24 plasmid was used as control (ctrl). Error bars represent one SD over three technical replicates.

(E) Relative Luciferase activity of the *Utf1*, *Jarid2* (enhancer 1 and 2), *Fgf5*, and *Prdm14* enhancer elements in serum as compared to the disrupted elements in 24 hr 2i. The empty pGL4.24 plasmid was used as control (ctrl). The number of scrambled nucleotides and total length of the tested elements are shown on the right. Error bars represent one SD over three technical replicates.

replaced identified OSN motifs with a scrambled sequence (see Experimental Procedures) and found that the activity of the elements was greatly impaired (Figure 2B, Figure S2A). To expand these findings, we next tested additional targets including *Utf1* and *Jarid2* (enhancer 1) as examples with no differential binding, *Fgf5* as an example of lower NANOG binding in 2i, and *Prdm14* and *Jarid2* (enhancer 2) representative of increased OSN binding (Figure 2C). In general we found that differential OSN binding was associated with altered activity of the tested elements in 2i (Figure 2D) and that all elements exhibited impaired activity upon disruption of the identified binding motifs (Figure 2E). Notably, control regions (no p300 enrichment in serum) did not alter their activity in 2i, and in the case of the *Otx2* promoter, the disruption of the OSN binding sites had no apparent effect on the activity either (Figures S2B and S2C).

OSN Rewiring Precedes the Global Loss of DNA Methylation in 2i

We next wanted to explore possible mechanisms that could lead to the global reorganization in transcription factor binding. As shown earlier H3K4me3 and H3K27me3 dynamics showed little overlap with changes in the OSN binding pattern (Figure 1F). As

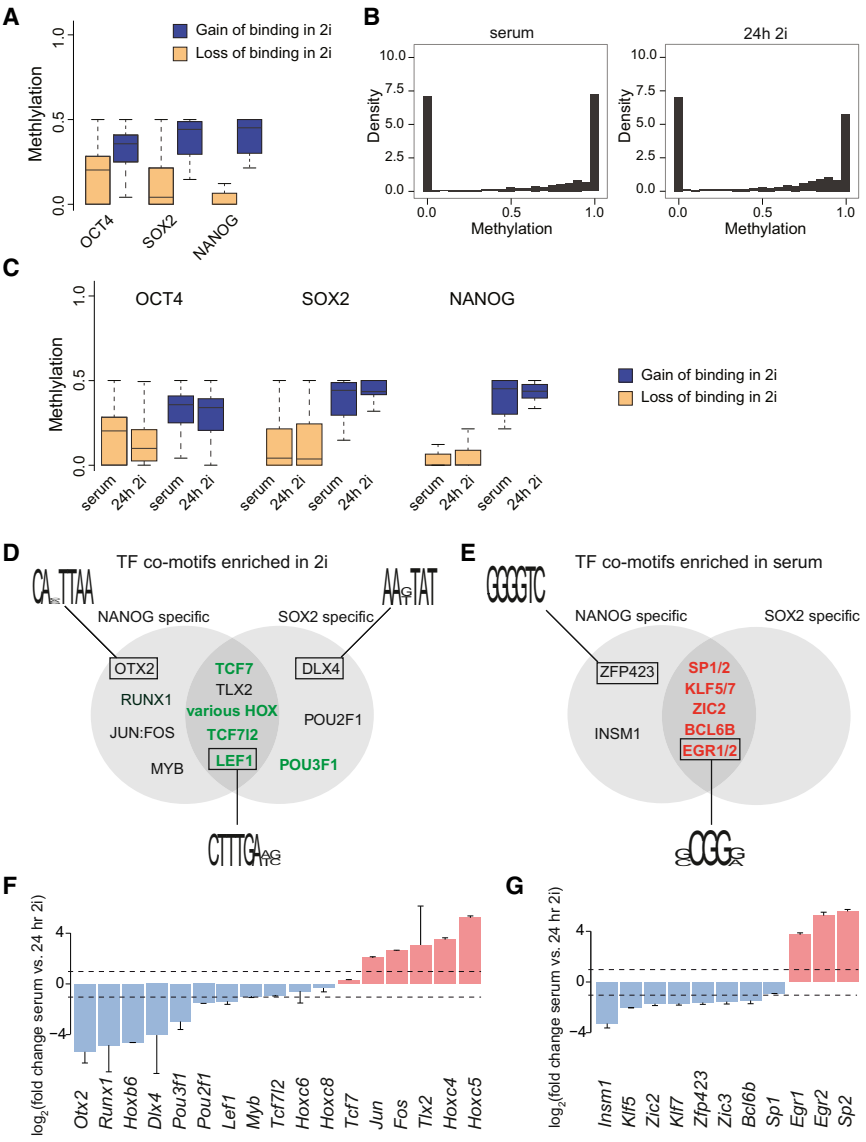

Figure 3. OSN Rewiring Precedes Global DNA Demethylation and Overlaps with Motifs of Factors Linked to Wnt and Erk Signaling

(A) DNA methylation levels of differentially bound OCT4, SOX2, and NANOG sites under serum conditions. Error bars represent one SD.

(B) Histograms showing the global DNA methylation distribution in mESCs (serum and 24 hr 2i).

(C) DNA methylation levels of differentially bound OCT4, SOX2, and NANOG sites in serum versus 24 hr 2i. Error bars represent one SD.

(D) Transcription factor motifs that are enriched in regions with increased binding for NANOG or SOX2 in 24 hr 2i. Transcription factors that are implicated in Wnt signaling are highlighted in green. Motifs exemplary for OTX2, LEF1, and DLX4 are shown.

(E) Transcription factor motifs that are enriched in regions with increased binding for NANOG or SOX2 in serum. Transcription factors that are implicated in Erk signaling are highlighted in red. Motifs exemplary for ZFP423 and EGR1/2 are shown.

(F) Expression ($\log_2$ fold change) of transcription factors in serum versus 24 hr 2i that were identified as co-factors for sites with higher NANOG and SOX2 binding in 2i. The error bars represent one SE over two biological replicates.

(G) Expression ($\log_2$ fold change) of transcription factors in serum versus 24 hr 2i that were identified as co-factors for sites with higher NANOG and SOX2 binding in serum. The error bars represent one SE over two biological replicates.

Differentially Bound OSN Sites Co-Occur with Motifs Linked to Wnt and Erk Signaling

Given the limited role of epigenetic modifications, we next looked into the occurrence of motifs that might point to relevant co-factors. We found that sites with increased binding in 2i are enriched for motifs corresponding to the transcription factors LEF1 and TCF7, which are direct effectors of the Wnt pathway (Reya and Clevers, 2005), as well as several HOX proteins whose expression is modulated through this pathway (Deschamps and van Nes, 2005) (Figure 3D). On the other hand, sites with decreased binding in 2i were specifically enriched for motifs of Erk pathway modulators, such as EGR1, SP1, and KLF7 (Black et al., 2001; Gregg and Fraizer, 2011; Merchant et al., 1999) (Figure 3E). Notably, several of the identified co-factors change their expression upon addition of the two kinase inhibitors (Figures 3F and 3G). This change in available co-factors might therefore impact the propensity of OSN to preferentially engage certain binding sites over others.

expected OSN sites that are bound in serum already exhibited low levels of DNA methylation (Figure 3A); however, sites that specifically gain OSN binding in 2i exhibit higher methylation levels in serum. To test whether the change in methylation is a cause or consequence of the differential binding, we measured global DNA methylation in serum versus 2i (24 hr). Importantly, in agreement with previous studies (Habibi et al., 2013; Ficz et al., 2013), we could not yet detect a global decrease in DNA methylation (Figure 3B). As a more site-specific loss of DNA methylation might be obscured in the global DNA methylation analysis, we next assessed the methylation status of regions with differential OSN binding after 24 hr in 2i, but we did not detect any change in DNA methylation in this analysis either (Figure 3C). In contrast, when we used published whole-genome bisulfite sequencing data to assess the intermediate transition state (7 days in 2i) and the adapted 2i population (GEO: GSE41923) we find that sites with a gain in OSN binding become subject to a gradual loss of methylation (Figure S3A).

Transcriptional Silencing of Bivalent Genes Is Independent of PRC2 Function in 2i

In line with previous reports (Marks et al., 2012), we find several bivalent loci such as the *HoxA* cluster or *Otx2* that exhibit a gradual loss of H3K27me3 (Figures 4A and 4B). However,

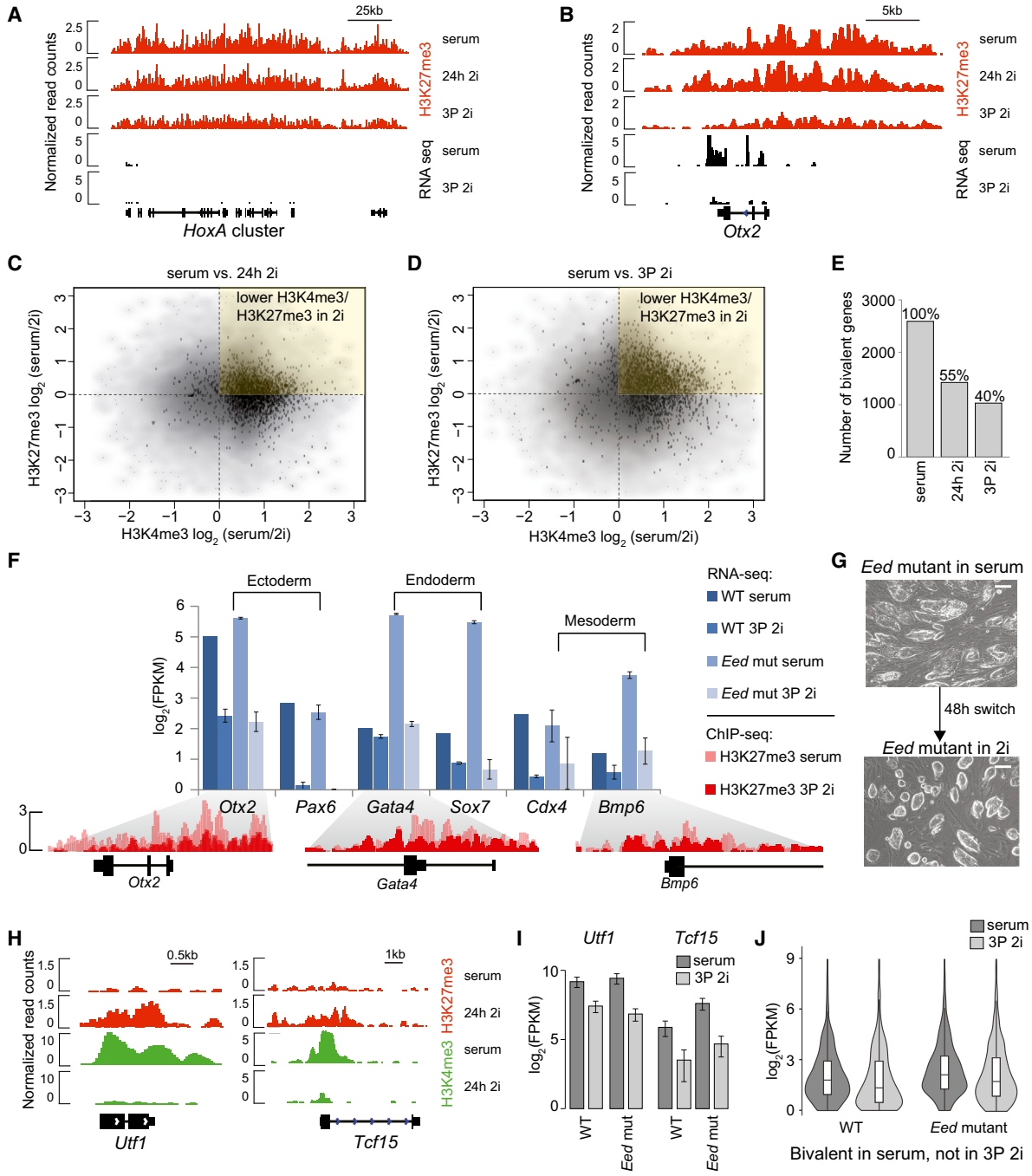

Figure 4. Transcriptional Silencing of Bivalent Genes Is Independent of PRC2 Function in 2i

(A) ChIP-seq tracks for H3K27me3 along the *HoxA* cluster in serum, 24 hr 2i, and 3P 2i, as well as RNA-seq tracks for serum and 3P 2i. Read counts are normalized to 1 million reads.

(B) ChIP-seq tracks for H3K27me3 along the *Otx2* gene locus in serum, 24 hr 2i, and 3P 2i, as well as RNA-seq tracks for serum and 3P 2i. Read counts are normalized to 1 million reads.

(C) Differentially enriched 1 kb tiles for H3K27me3 and H3K4me3 in serum versus 24 hr 2i. Bivalent loci are highlighted in black.

(D) Differentially enriched 1 kb tiles for H3K27me3 and H3K4me3 in serum versus 3P 2i. Bivalent loci are highlighted in black.

(E) Number of bivalent genes in serum, 24 hr 2i, and 3P 2i. Only 55% of genes that are bivalent in serum retain their bivalent status after 24 hr in 2i, which further decreases to 40% after 3P in 2i.

(F) Expression (log_2(FPKM)) for a selection of lineage markers in WT and *Eed* mutant cells in serum versus three passages 2i (3P). The transcriptional changes coincide with a decrease of H3K27me3 deposition along the promoter regions of the genes, as shown for the *Otx2*, *Gata4*, and *Bmp6* locus. The error bars represent one SE over two biological replicates.

(legend continued on next page)

both also show decreased H3K4me3 (Figures S4A and S4B) as reported previously (Gafni et al., 2013). When we plotted the global enrichment level of both histone modifications in serum versus 2i, we observed a general shift to lower enrichment for H3K4me3 at bivalent gene loci in the initial 2i transition, and this shift is largely maintained (Figures 4C and 4D). On the other hand, the repressive H3K27me3 mark shows a more subtle shift to lower enrichment within the first 24 hr in 2i, which becomes more pronounced after three passages. ChIP-qPCR further confirmed these subtle differences for H3K27me3 within the first 24 hr in 2i (Figure S4C). The faster H3K4me3 dynamics compared to H3K27me3 in this context are similar to observations in reprogramming (Koche et al., 2011). Overall, only 55% of all bivalent genes in serum retain their bivalent status after 24 hr in 2i and even fewer (40%) do so after three passages (Figure 4E, Table S4). However, similar to the *HoxA* cluster and *Otx2*, the differential enrichment of these histone marks seems to have little impact on the expression of associated genes (Figure S4D). This is consistent with previous reports showing that the basal expression level of many bivalent genes remains the same or is even further downregulated in 2i (Marks et al., 2012).

To better understand the relevance of H3K27me3 repression, we used an *Eed* mutant ESC line that is devoid of H3K27me3 (Montgomery et al., 2005) (Figure S4E). Under serum conditions, *Eed*-deficient cells are extremely unstable and display aberrant expression of differentiation-associated genes (Figure 4F), highlighting the importance of PRC2 function as a balancing factor in the metastable serum state (Boyer et al., 2006; Montgomery et al., 2005). However, when switched to 2i, the cells exhibited a complete morphologic and molecular stabilization, reflected by the abrogation of spontaneous differentiation and associated expression of differentiation genes (Figures 4F and 4G). Additionally, we find that *Utf1* and *Tcf15* de novo silencing—two genes that gain H3K27me3 early in the 2i transition—is unaffected despite the absence of H3K27me3 (Figures 4H and 4I). The same independence of PRC2-mediated silencing was observed in *Eed* knockdown cells (Figures S4F and S4G). Therefore the establishment of a repressed chromatin structure at the *Utf1* and *Tcf15* loci, albeit rapid in WT cells, can be interpreted as a secondary event in their transcriptional downregulation. To assess the generality of this finding, we generated RNA-seq data for *Eed* mutant cells in serum versus 2i (3P) and compared the expression profiles to those of the WT cells in serum versus 2i (3P). Interestingly, we find that PRC2-independent gene regulation is not limited to the loci mentioned above as the majority of differentially expressed genes becomes similarly induced or repressed in the absence of H3K27me3 (Figures S4H and S4I). Focusing on the differential expression of bivalent genes confirms this trend even further. The maintained or enforced repression of bivalent genes that lose their bivalent state in 2i (Table S4) highlights that many of these genes do not rely on a functioning PRC2 complex in 2i (Figure 4J).

Lastly, it has been shown that the protein PRDM14, a PR-domain-containing transcriptional regulator, is upregulated under 2i conditions and subsequently negatively regulates *Dnmt3a* and *Dnmt3b* expression (Leitch et al., 2013; Yamaji et al., 2013). Moreover, a previously published expression dataset suggests a negative correlation between the presence of PRDM14 and *Utf1* expression (Yamaji et al., 2013), which potentially accounts for the latter's repression in 2i. Again, as for WT cells, we detected a clear upregulation of *Prdm14* in the *Eed* mutant cells switched to 2i (Figure S4J). The previously postulated model suggested that PRDM14 exerts its repressive function through a direct recruitment of PRC2 to its target sites. However, we find that H3K27me3-deficient cells demonstrate uncompromised repression of *Dnmt3a/3b* as well as *Utf1*, suggesting that PRDM14 can either exert its function directly as a signaling regulator or operate through a different repressive mechanism (Figure 4I and Figure S4J). Taken together, these findings render PRC2-dependent dynamics of H3K27me3 a negligible variable in the explanation of transcriptional reconfiguration upon the transition to 2i.

DISCUSSION

The stable transition from serum/LIF to the 2i condition is associated with global transcriptional and epigenetic changes in ESCs. Key events in this transition constitute the upregulation of metabolism-associated genes, the downregulation of developmental-associated genes, and global hypomethylation of the cells, as well as a decline of the repressive histone mark H3K27me3 (Marks et al., 2012). Although a more homogenous distribution of NANOG points to a possible stabilization and reinforcement of the core pluripotency circuitry in 2i, the binding of the core pluripotency factors, OSN, in the transition to 2i have not been studied in detail. To fill this mechanistic gap, we focused on ESCs 24 hr after the switch and mapped the binding pattern of the core pluripotency factors OSN as well as the differential enrichment of the activating and repressive histone marks H3K4me3 and H3K27me3. While the core pluripotency factors show only moderate (*Nanog*) to no (*Oct4* and *Sox2*) differential expression in 2i, we detected a globally reconfigured binding pattern for all three factors after only 24 hr in 2i, highlighting their high sensitivity to altering ESC culturing conditions. Importantly, the early rewiring of OSN is largely maintained throughout the 2i transition and precedes the majority of changes in the enrichment of the bivalent chromatin marks H3K4me3 and H3K27me3 as well as the global loss of DNA methylation.

Although we find over one-third of all differentially expressed genes to be differentially bound in 2i, the overall correlation is

(G) Morphologic stabilization of *Eed* mutant cells in 2i. The cells exhibit a tight morphology together with the abrogation of spontaneous differentiation in 2i. Scale bar, 100 μm.
(H) ChIP-seq tracks for H3K27me3 and H3K4me3 along the *Utf1* and *Tcf15* locus in serum and after 24 hr in 2i. Read counts are normalized to 1 million reads.
(I) Expression (log_2(FPKM) of *Utf1* and *Tcf15* in serum versus 3P 2i in the WT and *Eed* mutant cells. The error bars represent one SE over two biological replicates.
(J) Violin plot showing the average expression (log_2(FPKM) for bivalent genes that lose their bivalent state both in 3P 2i (Table S4) in the WT in serum and 2i (3P) and in the *Eed* mutant line in serum and 2i (3P). Note that the average expression of bivalent genes decreases for the WT and the *Eed* mutant cells after three passages in 2i.

rather weak as the majority of differential binding events are not associated with expression changes. This result may not be that surprising as only a small subset of OSN-engaged genes are known to be bona fide targets while the majority are not affected by the depletion of any of the factors (Loh et al., 2006). Notably, this is a common phenomenon observed for transcription factors in higher eukaryotes where usually only 10%–25% of TF occupancy can be linked to expression of neighboring genes (Spitz and Furlong, 2012). Attributes that predict functional binding events are the presence of strong binding motifs and TF binding events at active enhancer elements (Cusanovich et al., 2014). Indeed, we find that the differential binding of the core pluripotency factors along key enhancer elements—but not at non-enhancer elements—correlates with their activity in 2i and that the disruption of identified OSN motifs results in a complete loss of enhancer activity. Although TF binding alone is not necessarily indicative of transcriptional activity, it might label regions that will be used subsequently, e.g., by stage-specific TFs (Spitz and Furlong, 2012). These priming events may therefore facilitate developmental transitions by reducing the rate-limiting step of chromatin remodeling. Interestingly, we find that differential binding sites are enriched for TF motifs associated with canonical Wnt signaling and the Erk pathway, the main signaling cascades perturbed through the inhibitors CHIR and PD, respectively. Specifically, sites with higher NANOG and SOX2 binding in 2i are enriched for motifs of TFs implicated in the 2i-enhanced Wnt signaling pathway, while sites with lower binding share motifs of cofactors involved in the differentiation-associated Erk signaling pathway, which is repressed in 2i. Thus, binding/priming of genes connected to differentiation is maintained in a metastable serum state, yet seems to be less crucial under enforced pluripotency conditions, where the engagement shifts to maintaining the pluripotent state.

Besides the rewiring of the core pluripotency network in 2i, we find that the divergent enrichment of the histone modifications H3K4me3 and H3K27me3 does not account for the majority of observed transcriptional variance in 2i. Moreover, H3K27me3-deficient *Eed* mutant cells induce normal repression of genes such as *Utf1* and *Tcf15* in 2i and maintained the silencing of bivalent loci. This dispensable function of PRC2 function in 2i is in contrast to the metastable serum/LIF state, which is highly dependent on proper PRC2 for maintenance of the pluripotent state (Geula et al., 2015). This apparent PRC2 independence in 2i is even more intriguing considering that this transition is also accompanied by global DNA hypomethylation (Ficz et al., 2013; Habibi et al., 2013). Therefore, 2i pluripotency—a state shielding ESCs from differentiation-inducing signals—appears to function in the absence of H3K27me3 and DNA methylation, both of which are generally regarded as key repressive epigenetic regulators in the metastable serum state. While more work remains to be done, our results further contribute to the understanding of the 2i state and regulation of pluripotency in general.

EXPERIMENTAL PROCEDURES

Cell Culture

mESCs were cultured in regular media containing 15% FBS, 1% PEN/STREP, 1% glutamine, 1% NEAA, and 5 × 10^5 U LIF. For ESC maintenance dishes were coated with 0.2% gelantin and irradiated CF1 mouse embryonic fibroblasts (MEFs) were plated as a confluent layer of feeder cells. ESCs were seeded in a density of 50,000 cells/6 wells and were split every 2–3 days. The 2i media was prepared according to the protocol of Ying et al. (2008) and was supplemented with 5 × 10^5 U LIF.

Antibodies

ChIP was performed using the following antibodies at a final concentration of 1 μg/1 × 10^6 cells: H3K4me3 (Millipore, 07-473), H3K27me3 (Millipore, 07-449), OCT4 (Santa Cruz, sc-8628 X), SOX2 (Santa Cruz, sc-17320 X), and NANOG (Cosmo Bio Ltd, REC-RCAB0002P-F). Immunostaining was done with the following primary antibodies, all diluted 1:1,000: NANOG (BD, 560259) and STELLA (Santa Cruz, sc-67249). Western blots were done using the following antibodies: UTF1 (1:1,000; Abcam, ab24273), Histone H3 (1:5,000; Abcam, ab61251), and EED (Abcam, ab4469).

ChIP

Cells were crosslinked in 1% formaldehyde for 15 min (5 min for UTF1 Antibody and UTF1-BioChIP) at room temperature, with constant agitation, and quenched with 125mM glycine for 5 min at room temperature. Nuclei were isolated and chromatin was sheared using Branson sonifier until the majority of DNA was in the range of 200–700 base pairs. Chromatin was incubated with antibody overnight at 4°C, with constant agitation. Immunoprecipitation of antibody-protein complexes was completed using Protein A or Protein G Dynabeads (Invitrogen) for 2–3 hr at 4°C, with constant agitation.

ACCESSION NUMBERS

The accession number for the ChIP-seq and RNA-seq data reported in this paper is GEO: GSE56312.

SUPPLEMENTAL INFORMATION

Supplemental Information for this article includes four figures, four tables, and Supplemental Experimental Procedures and can be found with this article online at http://dx.doi.org/10.1016/j.stem.2015.07.005.

AUTHOR CONTRIBUTIONS

C.G. conducted the experiments; C.G., M.Z., and A.M. conceived and designed the experiments; M.Z. performed computational analysis of ChIP-seq data; and R.K. performed computational analysis of RNA-seq and RRBS data. C.G., M.Z., and A.M. wrote the paper.

ACKNOWLEDGMENTS

We would like to thank Robbyn Issner, Holly Whitton, and Hongcang Gu for their advice and support regarding the ChIP-seq library preparation. A.M. is a New York Stem Cell Foundation, Robertson Investigator. This work was funded by the Human Frontiers Science Program, NIH grants 1P50HG006193 and P01GM099117, and the New York Stem Cell Foundation.

Received: March 12, 2014
Revised: March 25, 2015
Accepted: July 8, 2015
Published: July 30, 2015

REFERENCES

Black, A.R., Black, J.D., and Azizkhan-Clifford, J. (2001). Sp1 and krüppel-like factor family of transcription factors in cell growth regulation and cancer. J. Cell. Physiol. *188*, 143–160.

Boyer, L.A., Plath, K., Zeitlinger, J., Brambrink, T., Medeiros, L.A., Lee, T.I., Levine, S.S., Wernig, M., Tajonar, A., Ray, M.K., et al. (2006). Polycomb complexes repress developmental regulators in murine embryonic stem cells. Nature *441*, 349–353.

Buecker, C., Srinivasan, R., Wu, Z., Calo, E., Acampora, D., Faial, T., Simeone, A., Tan, M., Swigut, T., and Wysocka, J. (2014). Reorganization of enhancer patterns in transition from naive to primed pluripotency. Cell Stem Cell *14*, 838–853.

Chan, Y.S., Göke, J., Ng, J.H., Lu, X., Gonzales, K.A., Tan, C.P., Tng, W.Q., Hong, Z.Z., Lim, Y.S., and Ng, H.H. (2013). Induction of a human pluripotent state with distinct regulatory circuitry that resembles preimplantation epiblast. Cell Stem Cell *13*, 663–675.

Chen, X., Xu, H., Yuan, P., Fang, F., Huss, M., Vega, V.B., Wong, E., Orlov, Y.L., Zhang, W., Jiang, J., et al. (2008). Integration of external signaling pathways with the core transcriptional network in embryonic stem cells. Cell *133*, 1106–1117.

Creyghton, M.P., Cheng, A.W., Welstead, G.G., Kooistra, T., Carey, B.W., Steine, E.J., Hanna, J., Lodato, M.A., Frampton, G.M., Sharp, P.A., et al. (2010). Histone H3K27ac separates active from poised enhancers and predicts developmental state. Proc. Natl. Acad. Sci. USA *107*, 21931–21936.

Cusanovich, D.A., Pavlovic, B., Pritchard, J.K., and Gilad, Y. (2014). The functional consequences of variation in transcription factor binding. PLoS Genet. *10*, e1004226.

Deschamps, J., and van Nes, J. (2005). Developmental regulation of the Hox genes during axial morphogenesis in the mouse. Development *132*, 2931–2942.

Factor, D.C., Corradin, O., Zentner, G.E., Saiakhova, A., Song, L., Chenoweth, J.G., McKay, R.D., Crawford, G.E., Scacheri, P.C., and Tesar, P.J. (2014). Epigenomic comparison reveals activation of "seed" enhancers during transition from naive to primed pluripotency. Cell Stem Cell *14*, 854–863.

Ficz, G., Hore, T.A., Santos, F., Lee, H.J., Dean, W., Arand, J., Krueger, F., Oxley, D., Paul, Y.L., Walter, J., et al. (2013). FGF signaling inhibition in ESCs drives rapid genome-wide demethylation to the epigenetic ground state of pluripotency. Cell Stem Cell *13*, 351–359.

Gafni, O., Weinberger, L., Mansour, A.A., Manor, Y.S., Chomsky, E., Ben-Yosef, D., Kalma, Y., Viukov, S., Maza, I., Zviran, A., et al. (2013). Derivation of novel human ground state naive pluripotent stem cells. Nature *504*, 282–286.

Galonska, C., Smith, Z.D., and Meissner, A. (2014). In Vivo and in vitro dynamics of undifferentiated embryonic cell transcription factor 1. Stem Cell Reports *2*, 245–252.

Geula, S., Moshitch-Moshkovitz, S., Dominissini, D., Mansour, A.A., Kol, N., Salmon-Divon, M., Hershkovitz, V., Peer, E., Mor, N., Manor, Y.S., et al. (2015). Stem cells. m6A mRNA methylation facilitates resolution of naïve pluripotency toward differentiation. Science *347*, 1002–1006.

Gifford, C.A., Ziller, M.J., Gu, H., Trapnell, C., Donaghey, J., Tsankov, A., Shalek, A.K., Kelley, D.R., Shishkin, A.A., Issner, R., et al. (2013). Transcriptional and epigenetic dynamics during specification of human embryonic stem cells. Cell *153*, 1149–1163.

Gregg, J., and Fraizer, G. (2011). Transcriptional Regulation of EGR1 by EGF and the ERK Signaling Pathway in Prostate Cancer Cells. Genes Cancer *2*, 900–909.

Habibi, E., Brinkman, A.B., Arand, J., Kroeze, L.I., Kerstens, H.H., Matarese, F., Lepikhov, K., Gut, M., Brun-Heath, I., Hubner, N.C., et al. (2013). Whole-genome bisulfite sequencing of two distinct interconvertible DNA methylomes of mouse embryonic stem cells. Cell Stem Cell *13*, 360–369.

Kim, J., Chu, J., Shen, X., Wang, J., and Orkin, S.H. (2008). An extended transcriptional network for pluripotency of embryonic stem cells. Cell *132*, 1049–1061.

Koche, R.P., Smith, Z.D., Adli, M., Gu, H., Ku, M., Gnirke, A., Bernstein, B.E., and Meissner, A. (2011). Reprogramming factor expression initiates widespread targeted chromatin remodeling. Cell Stem Cell *8*, 96–105.

Kunath, T., Saba-El-Leil, M.K., Almousailleakh, M., Wray, J., Meloche, S., and Smith, A. (2007). FGF stimulation of the Erk1/2 signalling cascade triggers transition of pluripotent embryonic stem cells from self-renewal to lineage commitment. Development *134*, 2895–2902.

Leitch, H.G., McEwen, K.R., Turp, A., Encheva, V., Carroll, T., Grabole, N., Mansfield, W., Nashun, B., Knezovich, J.G., Smith, A., et al. (2013). Naive pluripotency is associated with global DNA hypomethylation. Nat. Struct. Mol. Biol. *20*, 311–316.

Loh, Y.H., Wu, Q., Chew, J.L., Vega, V.B., Zhang, W., Chen, X., Bourque, G., George, J., Leong, B., Liu, J., et al. (2006). The Oct4 and Nanog transcription network regulates pluripotency in mouse embryonic stem cells. Nat. Genet. *38*, 431–440.

Marks, H., Kalkan, T., Menafra, R., Denissov, S., Jones, K., Hofemeister, H., Nichols, J., Kranz, A., Stewart, A.F., Smith, A., and Stunnenberg, H.G. (2012). The transcriptional and epigenomic foundations of ground state pluripotency. Cell *149*, 590–604.

Merchant, J.L., Du, M., and Todisco, A. (1999). Sp1 phosphorylation by Erk 2 stimulates DNA binding. Biochem. Biophys. Res. Commun. *254*, 454–461.

Montgomery, N.D., Yee, D., Chen, A., Kalantry, S., Chamberlain, S.J., Otte, A.P., and Magnuson, T. (2005). The murine polycomb group protein Eed is required for global histone H3 lysine-27 methylation. Curr. Biol. *15*, 942–947.

Reya, T., and Clevers, H. (2005). Wnt signalling in stem cells and cancer. Nature *434*, 843–850.

Silva, J., Nichols, J., Theunissen, T.W., Guo, G., van Oosten, A.L., Barrandon, O., Wray, J., Yamanaka, S., Chambers, I., and Smith, A. (2009). Nanog is the gateway to the pluripotent ground state. Cell *138*, 722–737.

Spitz, F., and Furlong, E.E. (2012). Transcription factors: from enhancer binding to developmental control. Nat. Rev. Genet. *13*, 613–626.

Tesar, P.J., Chenoweth, J.G., Brook, F.A., Davies, T.J., Evans, E.P., Mack, D.L., Gardner, R.L., and McKay, R.D. (2007). New cell lines from mouse epiblast share defining features with human embryonic stem cells. Nature *448*, 196–199.

Yamaji, M., Ueda, J., Hayashi, K., Ohta, H., Yabuta, Y., Kurimoto, K., Nakato, R., Yamada, Y., Shirahige, K., and Saitou, M. (2013). PRDM14 ensures naive pluripotency through dual regulation of signaling and epigenetic pathways in mouse embryonic stem cells. Cell Stem Cell *12*, 368–382.

Yang, S.H., Kalkan, T., Morissroe, C., Marks, H., Stunnenberg, H., Smith, A., and Sharrocks, A.D. (2014). Otx2 and Oct4 drive early enhancer activation during embryonic stem cell transition from naive pluripotency. Cell Rep. *7*, 1968–1981.

Yeo, J.C., Jiang, J., Tan, Z.Y., Yim, G.R., Ng, J.H., Göke, J., Kraus, P., Liang, H., Gonzales, K.A., Chong, H.C., et al. (2014). Klf2 is an essential factor that sustains ground state pluripotency. Cell Stem Cell *14*, 864–872.

Ying, Q.L., Wray, J., Nichols, J., Batlle-Morera, L., Doble, B., Woodgett, J., Cohen, P., and Smith, A. (2008). The ground state of embryonic stem cell self-renewal. Nature *453*, 519–523.

Ziller, M.J., Gu, H., Müller, F., Donaghey, J., Tsai, L.T., Kohlbacher, O., De Jager, P.L., Rosen, E.D., Bennett, D.A., Bernstein, B.E., et al. (2013). Charting a dynamic DNA methylation landscape of the human genome. Nature *500*, 477–481.